

Pauli Paramagnetic Effects on Vortices in Superconducting $\text{TmNi}_2\text{B}_2\text{C}$

L. DeBeer-Schmitt,¹ M. R. Eskildsen,^{1,*} M. Ichioka,² K. Machida,² N. Jenkins,³
C. D. Dewhurst,⁴ A. B. Abrahamsen,⁵ S. L. Bud'ko,⁶ and P. C. Canfield⁶

¹*Department of Physics, University of Notre Dame, Notre Dame, Indiana 46556, USA*

²*Department of Physics, Okayama University, Okayama 700-8530, Japan*

³*DPMC, University of Geneva, 24 Quai E.-Ansermet, CH-1211 Genève 4, Switzerland*

⁴*Institut Laue-Langevin, 6 Rue Jules Horowitz, F-38042 Grenoble, France*

⁵*Materials Research Department, Risø National Laboratory, DK-4000 Roskilde, Denmark*

⁶*Ames Laboratory and Department of Physics and Astronomy, Iowa State University, Ames, Iowa 50011, USA*

(Dated: November 4, 2018)

The magnetic field distribution around the vortices in $\text{TmNi}_2\text{B}_2\text{C}$ in the paramagnetic phase was studied experimentally as well as theoretically. The vortex form factor, measured by small-angle neutron scattering, is found to be field independent up to $0.6H_{c2}$ followed by a sharp decrease at higher fields. The data are fitted well by solutions to the Eilenberger equations when paramagnetic effects due to the exchange interaction with the localized $4f$ Tm moments are included. The induced paramagnetic moments around the vortex cores act to maintain the field contrast probed by the form factor.

PACS numbers: 74.25.Op, 74.25.Ha, 74.70.Dd, 61.12.Ex

The interplay between superconductivity and local magnetic moments is a fascinating problem, with relevance to a number of important unresolved questions such as the detailed nature of both high- T_c and heavy-fermion superconductivity. Adding to this the usually antagonistic nature of superconductivity and magnetism, it is no surprise that materials which exhibit a coexistence of these two groundstates attract a lot of attention.

The antiferromagnetic members of the intermetallic nickelborocarbide superconductors $R\text{Ni}_2\text{B}_2\text{C}$ ($R = \text{Ho}$, Er or Tm) have proved especially rich vehicles for such studies, displaying *e.g.* intertwined magnetic and superconducting transitions as well as subtle changes in the superconducting characteristic length scales associated with the onset of antiferromagnetic ordering [1, 2, 3]. The exchange interaction $\mathcal{H}_{sf} = -I(g_J - 1)\mathbf{J} \cdot \mathbf{s}$ between the $4f$ localized moment \mathbf{J} and the conduction electron spin \mathbf{s} (g_J is Landé g -factor and I is exchange integral) is important in understanding systematic changes of both superconducting and magnetic transition temperatures [4]. However, even in the paramagnetic state above the antiferromagnetic ordering temperature, T_N , the conduction electron moment $\boldsymbol{\mu}_e = g\mu_B\mathbf{s}$ is subjected to an exchange field $\mathbf{H}_{\text{ex}} = I(g_J - 1)\mathbf{J}/g\mu_B$ due to the field induced $4f$ -moments, yielding a “Zeeman” term $\mathcal{H}_{sf} = -\mathbf{H}_{\text{ex}} \cdot \boldsymbol{\mu}_e$ in the conduction electron Hamiltonian.

Here we report on combined experimental and theoretical studies of $\text{TmNi}_2\text{B}_2\text{C}$, investigating specifically how the magnetic field profile around the vortices is influenced by the paramagnetic state. Using small-angle neutron scattering (SANS) we imaged the vortex lattice (VL) at several temperatures $> T_N$, and measured the magnetic field dependence of the form factor which reflects the field distribution around the vortices. In contrast to the usual exponential decrease with increasing field, the VL form

factor in $\text{TmNi}_2\text{B}_2\text{C}$ remains constant up to $H \sim 0.6H_{c2}$, followed by a sudden decrease as the upper critical field is approached. It is the striking departure from exponential behavior which is the central result of this Letter.

The experimental results are compared to solutions of the quasi-classical Eilenberger equations, focusing on how the internal field distribution in the mixed state is affected by changes to the electronic vortex core structure due to the paramagnetism. Since $M(H)$ is roughly linear below H_{c2} [5] the induced moment \mathbf{J} is proportional to the applied field and can thus be treated as an effective Pauli paramagnetic effect, giving rise to a Zeeman energy μB where the parameter μ signifies the strength of the paramagnetic effect. The calculations show how the induced moments in and around the vortices grow with increasing applied field and thereby maintaining a high field modulation (and hence form factor), before they eventually spread out from the core region at high fields. The results of the calculations provide an excellent quantitative agreement with the measured form factor.

$\text{TmNi}_2\text{B}_2\text{C}$ has a superconducting critical temperature, $T_c = 11$ K, and the Tm moments order antiferromagnetically in a long-period transverse-modulated state below $T_N = 1.5$ K [1, 5, 6, 7]. At low temperature the magnetic moments are along the c axis, which consequently is the direction of the maximum magnetic susceptibility [5, 6]. For magnetic fields applied parallel to the c axis H_{c2} shows a non-monotonic behavior, reaching a maximum near $T = 5$ K and $\mu_0 H_{c2} = 1$ T due to the Tm sublattice magnetization, decreasing upon approaching the magnetic ordering temperature and finally increasing again below T_N [1, 5]. Previous studies showed simultaneous magnetic and VL symmetry transitions below T_N , as well as peaks in the FLL reflectivity associated with the magnetic transitions [1].

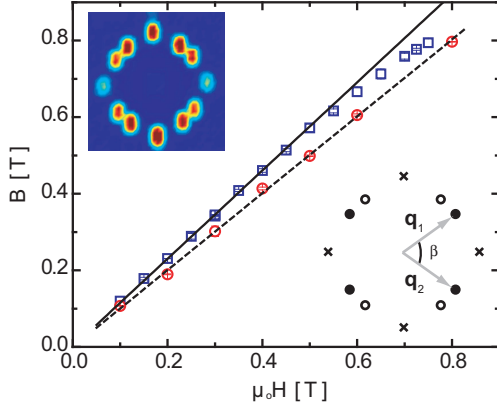


FIG. 1: (Color online) Measured magnetic induction versus applied field at 1.6 K for TmNi₂B₂C (squares) and non-magnetic LuNi₂B₂C (circles). The top left inset show a VL diffraction pattern obtained at 0.2 T and 1.6 K. The bottom right inset show a schematic of the diffraction pattern, indicating the VL scattering vectors and opening angle. Open and closed circles represent peaks belonging to different domain orientations, while ×'s denote higher order reflections.

SANS experiments were carried out at the D11 instrument at the Institut Laue-Langevin. The TmNi₂B₂C single crystal used in the experiment was grown using a high temperature flux method, using isotopically enriched ¹¹B to reduce neutron absorption [8]. Incident neutrons with wavelengths of $\lambda_n = 6 - 8$ Å and a wavelength spread of $\Delta\lambda_n/\lambda_n = 10\%$ were used. The VL diffraction pattern was collected by a position sensitive detector. For all measurements, the sample was cooled in a horizontal magnetic field applied parallel to the crystalline *c* axis and the incoming neutrons. Measurements obtained at zero field were used for background subtraction.

The VL was imaged as a function of field at temperatures, $T = 1.6$ K, 3.5 K and 5.0 K. At all fields and temperatures a rhombic VL was observed, as shown in the insets to Fig. 1. The opening angle, β , was found to decrease with increasing field indicating a continuous transition from a distorted square to a distorted hexagonal symmetry in agreement with previous reports [1]. As a consequence of having a non-square VL pinned to an underlying square crystalline lattice, two VL domains were observed at all measured fields and temperatures.

A direct measure of the magnetic induction, B , in the sample can be obtained from the VL scattering vectors. Using two scattering vectors belonging to the same domain, the induction is given by

$$B = \frac{\phi_0}{4\pi^2} |\mathbf{q}_1 \times \mathbf{q}_2|, \quad (1)$$

where $\phi_0 = 20.7 \times 10^4$ TÅ² is the flux quantum. Fig. 1 shows the measured induction as a function of applied field for TmNi₂B₂C. To rule out the possibility of systematic errors on the determination of B , measure-

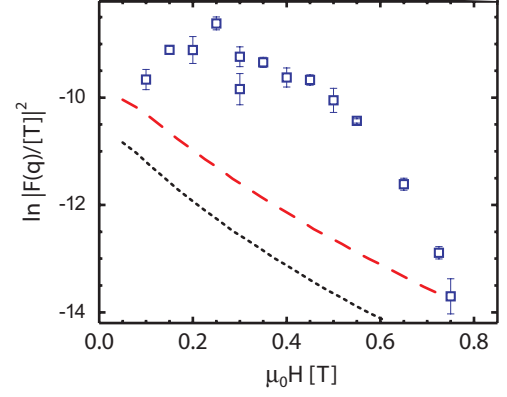


FIG. 2: (Color online) Field dependence of the measured VL form factor in TmNi₂B₂C at 1.6 K. The lines show the form factor calculated using eqn. (3) with $\xi = 210$ Å and $\lambda = 780$ Å (dotted line) or 600 Å (dashed line).

ments on non-magnetic LuNi₂B₂C were performed immediately prior to the measurements on TmNi₂B₂C using the same instrumental configuration. The measurements on LuNi₂B₂C yielded $dB/d(\mu_0 H) = 1.003 \pm 0.006$ (dashed line) as expected for a non-magnetic superconductor when $H \gg H_{c1}$. For TmNi₂B₂C we find $B > \mu_0 H$ for the entire measured field range as seen in Fig. 1, indicating a significant paramagnetic contribution to the induction. Below ~ 0.6 T, $dB/d(\mu_0 H) = 1.152 \pm 0.004$ as indicated by the straight line in Fig. 1. Taking demagnetization effects into account, this is in excellent agreement with magnetization measurements [5]. At higher fields B approaches $\mu_0 H$, with the two fields seemingly merging at $\mu_0 H_{c2} \approx 0.75$ T. We do presently not have an explanation for the high field behavior of B .

We now turn to the main focus of this Letter: Measurements of the TmNi₂B₂C VL form factor, $F(q)$, which is the Fourier transform of the magnetic field modulation due to the vortices. Experimentally the form factor is related to the VL reflectivity by

$$R = \frac{2\pi\gamma^2\lambda_n^2 t}{16\phi_0^2 q} |F(q)|^2, \quad (2)$$

where $\gamma = 1.91$ is the neutron gyromagnetic ratio, t is the sample thickness, and q is the magnitude of the scattering vector [9]. Fig. 2 shows the VL form factor for TmNi₂B₂C at 1.6 K just above T_N , obtained from the integrated intensity of the Bragg peaks, as the sample is rotated through the diffraction condition.

Using the model obtained by Clem and valid for $\kappa_{GL} = \lambda/\xi \gg 1$ [10]:

$$F(q) = B \frac{g K_1(g)}{1 + \lambda^2 q^2}, \quad g = \sqrt{2}\xi (q^2 + \lambda^{-2})^{1/2}, \quad (3)$$

where K_1 is a modified Bessel function, we have calculated expected vortex form factors shown by in Fig. 2.

The dotted line corresponds to a penetration depth, $\lambda = 780$ Å from literature [5] and a coherence length based on the upper critical field at 1.6 K, $\xi_{c2} = \sqrt{\phi_0/2\pi H_{c2}} = 210$ Å. As it is evident, the calculated form factor falls substantially below our inferred values. Using a somewhat smaller value of the penetration depth, $\lambda = 600$ Å (dashed line), yields a better fit to the endpoints of the measured form factor, but fails to describe the non-exponential field dependence at all intermediate fields. Qualitatively similar results were also obtained at temperatures further above T_N as shown in Fig. 3. As we will show below the unusual field dependence of the form factor can be explained by a microscopic calculation taking into account paramagnetic effects which modify the magnetic field profile around the vortices.

The form factor $F(\mathbf{q}_{h,k})$ is calculated from the internal field distribution $B(\mathbf{r}) = \sum_{h,k} F(\mathbf{q}_{h,k}) \exp(i\mathbf{q}_{h,k} \cdot \mathbf{r})$ with the wave vector $\mathbf{q}_{h,k} = h\mathbf{q}_1 + k\mathbf{q}_2$, $\mathbf{q}_1 = (2\pi/a, -\pi/a_y, 0)$ and $\mathbf{q}_2 = (2\pi/a, \pi/a_y, 0)$, corresponding to VL unit vectors $(a/2, a_y)$ and $(a/2, -a_y)$. The intensity of the main peak at $(h, k) = (1, 0)$ gives the fundamental component $F(\mathbf{q}_{0,1})$. To determine $B(\mathbf{r})$ we selfconsistently calculate the spatial structure of the pair potential $\Delta(\mathbf{r})$ and the vector potential $\mathbf{A}(\mathbf{r})$ using the quasiclassical Eilenberger theory in the clean limit [11, 12, 13, 14, 15, 16], including the paramagnetic contribution due to the effective Zeeman effect through the exchange coupling of the conduction electron and TmNi₂B₂C sublattice moments. The quasi-classical Green's functions $g(\omega_n, \mathbf{k}, \mathbf{r})$, $f(\omega_n, \mathbf{k}, \mathbf{r})$, and $f^\dagger(\omega_n, \mathbf{k}, \mathbf{r})$ are calculated in the vortex lattice state by the Eilenberger equations

$$\begin{aligned} \{\omega_n + i\mu B + \mathbf{k} \cdot (\nabla + i\mathbf{A})\} f &= \Delta \phi(\mathbf{k}) g, \\ \{\omega_n + i\mu B - \mathbf{k} \cdot (\nabla - i\mathbf{A})\} f^\dagger &= \Delta^* \phi^*(\mathbf{k}) g, \end{aligned} \quad (4)$$

with $g = (1 - f f^\dagger)^{1/2}$, $\text{Re}\{g\} > 0$, the pairing function $\phi(\mathbf{k})$, Matsubara frequency $\omega_n = (2n + 1)\pi T$, and effective Zeeman energy μB [16]. Here μ determines the strength of the paramagnetic effect. A simple two-dimensional Fermi surface is used, with a Fermi momentum unit vector given by $\mathbf{k} = (\cos \theta, \sin \theta)$ and $0 \leq \theta < 2\pi$. With the magnetic field applied along the z axis direction, the vector potential $\mathbf{A}(\mathbf{r}) = \frac{1}{2} \bar{\mathbf{B}} \times \mathbf{r} + \mathbf{a}(\mathbf{r})$ in the symmetric gauge, where $\bar{\mathbf{B}} = (0, 0, \bar{B})$ is the average, uniform flux density and $\mathbf{a}(\mathbf{r})$ is related to the modulated internal field such that $\mathbf{B}(\mathbf{r}) = \bar{\mathbf{B}} + \nabla \times \mathbf{a}(\mathbf{r})$.

The selfconsistent conditions for $\Delta(\mathbf{r})$ and $\mathbf{A}(\mathbf{r})$ are given by respectively

$$\Delta = g_0 N_0 T \sum_{0 < \omega_l \leq \omega_{\text{cut}}} \left\langle \phi^*(\mathbf{k}) \left(f + f^\dagger \right) \right\rangle_{\mathbf{k}}, \quad (5)$$

and

$$\nabla \times (\nabla \times \mathbf{A}) = \nabla \times \mathbf{M}_{\text{para}} - \frac{2T}{\kappa^2} \sum_{0 < \omega_l} \langle \mathbf{k} \text{Im}\{g\} \rangle_{\mathbf{k}}, \quad (6)$$

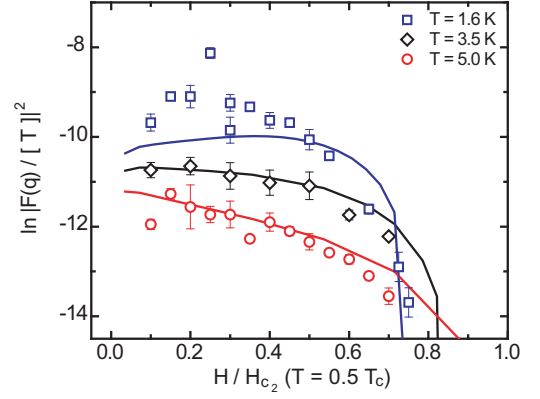


FIG. 3: (Color online) Comparison of measured and calculated VL form factors in TmNi₂B₂C at $T = 1.6, 3.5$, and 5.5 K. The curves were calculated using the model described in the text, for $T = 0.16T_c$ and $\mu = 1.71$ (A), $T = 0.35T_c$ and $\mu = 1.28$ (B), and $T = 0.50T_c$ and $\mu = 0.86$ (C).

where $\langle \dots \rangle_{\mathbf{k}}$ indicates the Fermi surface average, and $\kappa = \sqrt{7\zeta(3)/8\kappa_{\text{GL}}} \sim \kappa_{\text{GL}}$ where κ_{GL} is the Ginzburg-Landau (GL) parameter [17]. In Eq. (5), $(g_0 N_0)^{-1} = \ln T + 2T \sum_{0 < \omega_l \leq \omega_{\text{cut}}} \omega_l^{-1}$, and we use $\omega_{\text{cut}} = 20k_B T_c$. In Eq. (6) both the diamagnetic contribution of supercurrent in the last term and the contribution of the paramagnetic moment $\mathbf{M}_{\text{para}} = (0, 0, M_{\text{para}}(\mathbf{r}))$ with

$$M_{\text{para}}(\mathbf{r}) = \left(\frac{\mu}{\kappa} \right)^2 \left(B(\mathbf{r}) - \frac{2T}{\mu} \sum_{0 < \omega_l} \langle \text{Im}\{g\} \rangle_{\mathbf{k}} \right), \quad (7)$$

are treated fully self-consistently [16]. As mentioned earlier, the vortices in TmNi₂B₂C at low temperature and intermediate fields form a distorted square VL [1], indicating a large fourfold anisotropy of the Fermi surface and pairing function [18]. We consequently use a pairing function $\phi(\mathbf{k}) = |\sqrt{2} \cos 2\theta|$ and a square VL configuration ($a_y = a/2$). However, the overall qualitative features of the form factor do not depend much on these choices.

The field dependence of the calculated $|F(\mathbf{q} = \mathbf{q}_{0,1})|$ is shown in Fig. 3, where we have used $\mu_0 H_{c2}(T = 0.5T_c) = 1$ T for comparison with the experimental data. The magnitude of $|F(q)|^2$ depends on the GL parameter, and its gradient as a function of field is related to the paramagnetic parameter μ . At $T = 0.5T_c$ (5 K) values for $\kappa = 6.2$ and $\mu = 0.86$ were chosen to obtain agreement between the calculated and measured form factor at low and intermediate fields. The small deviation close to H_{c2} may be due to the increasing deformation of the VL away from a square symmetry [1], which is not included in this calculation. While κ is kept constant for the remainder of the calculations, the value of μ is expected to be proportional to the magnetization which in TmNi₂B₂C is dominated by the contribution from the Tm $4f$ -moments [5]. The decrease of H_{c2} below 5 K can thus be attributed to an increasing paramagnetic depairing. We therefore

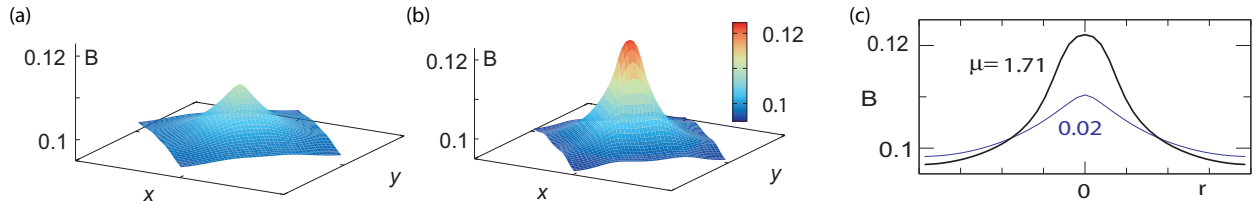


FIG. 4: (Color online) Spatial structure of internal field $B(\mathbf{r})$ within a unit cell of the square vortex lattice. Here $\bar{B} = 0.1 = 0.36H_{c2}(0.5T_c)$, $\kappa = 6.2$, $T = 0.16T_c$, and $\mu = 0.02$ (a) and 1.71 (b). A profile of the field distribution is shown in (c).

determine values of μ such that they reproduce the suppression of $H_{c2}(T)$, yielding $\mu = 1.28$ at $T = 0.35T_c$ (3.5 K) and $\mu = 1.71$ at $T = 0.16T_c$ (1.6 K), corresponding to respectively $H_{c2}(T)/H_{c2}(0.5T_c) \sim 0.85$ and 0.75 . As a consequence of the increasing value of μ , the slope of the form factor at low fields changes from negative to positive (curves $C \rightarrow B \rightarrow A$ in Fig. 3). As evident from Fig. 3 the calculated form factor at $0.35T_c$ provides a good fit to the experimental data. At $0.16T_c$ the calculated form factor captures the qualitative field dependence, but falls below the datapoints at low fields. The reason for this quantitative deviation is not clear, but it may be related to critical behavior due to the close proximity to T_N .

The paramagnetic moments induced around the vortex cores enhance $B(\mathbf{r})$, and consequently also the form factor $|F(\mathbf{q}_{01})|$ which acquires a paramagnetic component proportional to H . To visualize the contribution from the paramagnetic moments around the vortex cores, Fig. 4 shows the spatial structure of the internal field $B(\mathbf{r})$ in a VL unit cell for $\mu = 0.02$ (a) and 1.71 (b). The vortex field profile along the nearest neighbor direction is plotted in Fig. 4(c). This shows how the paramagnetic component is confined at the vortex center resulting in the enhancement of the internal field.

Before concluding we would like to emphasize the relative “simplicity” of $\text{TmNi}_2\text{B}_2\text{C}$ as well as the theoretical model used here to describe the SANS results. In contrast to the d - or (triplet) p -wave pairing observed in respectively the high T_c ’s and SrRuO_4 [19] the Cooper pairs in $\text{TmNi}_2\text{B}_2\text{C}$ are singlets with only a modest gap anisotropy [20]. Likewise Pauli paramagnetic limiting and a possible non-uniform superconducting (FFLO) state which have recently received considerable attention in the heavy fermion superconductor CeCoIn_5 [21] is not relevant in the case of $\text{TmNi}_2\text{B}_2\text{C}$ [22]. Instead we argue that one can consider $\text{TmNi}_2\text{B}_2\text{C}$ as a “standard” paramagnetic (above T_N) superconductor, thus providing a very valuable reference for more exotic materials.

In summary, we have presented combined experimental and theoretical studies of vortices and the vortex lattice in $\text{TmNi}_2\text{B}_2\text{C}$ in the paramagnetic phase above T_N . The physical picture which emerges is that the conduction electron paramagnetic moments induced by the exchange interaction accumulate exclusively around the vortex cores, creating nano-tubes of Tm magnetization

and maintaining the field distribution contrast of the VL. While our calculation used a simple model to describe the H - and T -dependences, it was still able to capture the qualitative and quantitative behavior of the form factor, emphasizing that paramagnetic effects are important in understanding the vortex state in $\text{TmNi}_2\text{B}_2\text{C}$.

After submission we became aware of a theoretical paper by J. Jensen and P. Hedegård (to be published in Phys. Rev. B) which also treats the anomalous field dependence of the form factor in $\text{TmNi}_2\text{B}_2\text{C}$.

We are grateful to V. G. Kogan for numerous stimulating discussions. MRE acknowledges support by the Alfred P. Sloan Foundation. Work at Ames Laboratory is supported by the U. S. Department of Energy, Basic Energy Sciences under Contract No. W-7405-Eng-82.

* Electronic address: eskildsen@nd.edu

- [1] M. R. Eskildsen *et al.*, Nature (London) **393**, 242 (1998).
- [2] P. L. Gammel *et al.*, Phys. Rev. Lett. **82**, 1756 (1999).
- [3] K. Nørgaard *et al.*, Phys. Rev. Lett. **84**, 4982 (2000).
- [4] See for example, K. Machida, K. Nokura and T. Matsubara, Phys. Rev. B **22**, 2307 (1980).
- [5] B. K. Cho *et al.*, Phys. Rev. B **52**, 3676 (1995).
- [6] J. Lynn *et al.*, Phys. Rev. B **55**, 6584 (1997).
- [7] B. Sternlieb *et al.*, J. Appl. Phys. **81**, 4937 (1997).
- [8] P. C. Canfield and I. R. Fisher, J. Crystal Growth **225**, 155 (2001).
- [9] D. K. Christen *et al.*, Phys. Rev. B **15**, 4506 (1977).
- [10] J. Clem, J. Low Temp. Phys. **18**, 427 (1975).
- [11] G. Eilenberger, Z. Phys. **214**, 195 (1968).
- [12] U. Klein, J. Low Temp. Phys. **69**, 1 (1987).
- [13] M. Ichioka *et al.*, Phys. Rev. B **70**, 144508 (2004).
- [14] U. Klein, D. Rainer, and H. Shimahara, J. Low Temp. Phys. **118**, 91 (2000).
- [15] K. Watanabe, T. Kita, and M. Arai, Phys. Rev. B **71**, 144515 (2005).
- [16] M. Ichioka *et al.*, Phys. Rev. B **76**, 014503 (2007).
- [17] P. Miranovic and K. Machida, Phys. Rev. B **67**, 092506 (2003).
- [18] N. Nakai *et al.*, Phys. Rev. Lett. **89**, 237004 (2002).
- [19] See e.g. Y. Maeno, T. M. Rice, and M. Siegrist, Physics Today **54**(1), 42 (2001) and references therein.
- [20] H. Suderow *et al.*, Phys. Rev. B **64**, 020503(R) (2001).
- [21] For a recent review see Y. Matsuda and H. Shimahara, J. Phys. Soc. Jpn. **76**, 051005 (2007).
- [22] The orbital critical field in $\text{TmNi}_2\text{B}_2\text{C}$ estimated from

$(dH_{c2}/dT)|_{T_c}$ yields $H_{c2}^{\text{orb}} = 2.1 \text{ T}$ [5], an order of magnitude smaller than the Pauli limiting field $H_{c2}^{\text{P}} = \sqrt{2}\Delta(0)/g\mu_B \approx 17.7 \text{ T}$ obtained using $\Delta(0) = 1.45 \text{ meV}$ [20, 21].